COMMUNICATION

ADVANCED MATERIALS

Lithium–Sulfur Batteries

www.advmat.de

A Polysulfide-Immobilizing Polymer Retards the Shuttling of Polysulfide Intermediates in Lithium–Sulfur Batteries

Shuibin Tu, Xiang Chen, Xinxin Zhao, Mingren Cheng, Peixun Xiong, Yongwu He, Qiang Zhang, and Yunhua Xu**

Lithium–sulfur batteries are regarded as one of the most promising candidates for next-generation rechargeable batteries. However, the practical application of lithium–sulfur (Li–S) batteries is seriously impeded by the notorious shuttling of soluble polysulfide intermediates, inducing a low utilization of active materials, severe self-discharge, and thus a poor cycling life, which is particularly severe in high-sulfur-loading cathodes. Herein, a polysulfide-immobilizing polymer is reported to address the shuttling issues. A natural polymer of Gum Arabic (GA) with precise oxygen-containing functional groups that can induce a strong binding interaction toward lithium polysulfides is deposited onto a conductive support of a carbon nanofiber (CNF) film as a polysulfide shielding interlayer. The as-obtained CNF–GA composite interlayer can achieve an outstanding performance of a high specific capacity of 880 mA h g^{-1} and a maintained specific capacity of 827 mA h g^{-1} after 250 cycles under a sulfur loading of 1.1 mg cm^{-2}. More importantly, high reversible areal capacities of 4.77 and 10.8 mA h cm^{-2} can be obtained at high sulfur loadings of 6 and even 12 mg cm^{-2}, respectively. The results offer a facile and promising approach to develop viable lithium–sulfur batteries with high sulfur loading and high reversible capacities.

With the rapid development of hand-held electronic devices and electric vehicles, high-power, and high-energy-density energy storage systems have been capturing extensive witnesses and ever-increasing research enthusiasm. Lithium–sulfur (Li–S) batteries are considered as a promising candidate for next-generation rechargeable batteries due to their high theoretical energy density (2600 Wh kg^{-1}).[1,2] In addition, sulfur possesses distinct advantages, such as being cost effective, nontoxic, and having abundant natural resource.[3,4] Nevertheless, the practical application of Li–S batteries is hindered by several challenges. The predominant one is the shuttling of soluble polysulfides between sulfur cathodes and lithium metal anodes, which induces irreversible loss of active materials, severe self-discharge, low Coulombic efficiency, and poor cycling stability.[5–8]

Tremendous efforts have been devoted to suppressing the shuttling of polysulfides to enlarge the lifespan of Li–S batteries, including designing sulfur composites,[7,9–15] optimizing electrolytes,[16–18] polysulfide anchoring binders,[19–21] and stabilizing lithium metal anodes.[22–26] Although these methods greatly improve the electrochemical performance of Li–S batteries, the shuttle effect still exists in a working cell. Recently, functional separators/interlayers have been reported to serve as a promising strategy to address the shuttle effect through immobilizing polysulfides on functional separators and/or confining them within the sulfur cathode side. For instance, Su and Manthiram employed a carbon nanotube paper as a functional interlayer to hinder the soluble polysulfides, which remarkably improved the electrochemical performance of Li–S batteries.[27] However, the carbon nanotube interlayer only acts as a physical barrier, which is insufficient to suppress the shuttling behavior. Afterward, various functional separators/interlayers were proposed, including coating Nafion on separators to block the migration of polysulfides anions via electrostatic repulsion[28,29] and using metal–organic framework (MOF) or graphene interlayers as ionic sieves to suppress the diffusion of the soluble polysulfides.[30–32] However, these improvements are mostly based on relatively low-sulfur-loading cathodes because of their intrinsically sluggish electrical

---

S. B. Tu, X. X. Zhao, M. R. Cheng, P. X. Xiong, Y. W. He, Prof. Y. H. Xu
School of Materials Science and Engineering
Key Laboratory of Advanced Ceramics and Machining Technology
(Ministry of Education)
Tianjin Key Laboratory of Composite and Functional Materials
and Tianjin Key Laboratory of Molecular Optoelectronic Science
Tianjin University
Tianjin 300072, China
E-mail: yunhua.xu@tju.edu.cn

X. Chen, Prof. Q. Zhang
Beijing Key Laboratory of Green Chemical Reaction Engineering
and Technology
Department of Chemical Engineering
Tsinghua University
Beijing 100084, China
E-mail: zhang-qiang@mails.tsinghua.edu.cn

Prof. Y. H. Xu
Collaborative Innovation Center of Chemical Science
and Engineering (Tianjin)
Tianjin 300072, China

The ORCID identification number(s) for the author(s) of this article can be found under https://doi.org/10.1002/adma.201804581.

DOI: 10.1002/adma.201804581

and/or Li$^+$ ionic conductivity. To further address the shuttle effect at high sulfur loading, Zheng and co-workers described a functional separator by filtrating 2D porous nitrogen-doped carbon nanosheets on a polypropylene (PP) separator and demonstrated the significant suppression of polysulfide shuttling.[33] However, the fabrication process of such functional coating layer is very complicated. Therefore, it is still very challenging to afford a practical strategy to simultaneously improve the cycling performance and sulfur loading of Li–S batteries.

In this contribution, Gum Arabic (GA), a natural and widely used polymer, is introduced to conductive carbon nanofiber (CNF) networks to build free-standing CNF–GA composite films via a solution-coating method. The GA is mainly composed of highly branched polysaccharides, consisting of a galactan backbone chain with heavily branched galactose, arabinose, rhamnose, and hydroxyproline side chains that can afford a strong binding interaction toward lithium polysulfides (LiPSs) through its rich hydroxyl, carboxyl, and ether functional groups.[34–36] The as-obtained CNF–GA composite films can thus effectively impede the shuttle effect. In addition, the conductive composite films, functioned as upper current collectors, can improve the sulfur utilization, ensuring a compatibility with high-sulfur-loading cathodes. With CNF–GA interlayers, the sulfur cathodes demonstrated a good cyclability with a capacity retention of 94% over 250 cycles, an outstanding hinder self-discharge capability, superb rate performance, and a high reversible areal capacity of 10.8 mA h cm^{-2} upon a high sulfur loading of 12 mg cm^{-2}, which outperform the state-of-the-art lithium-ion batteries (≈4 mA h cm^{-2}) and most Li–S batteries reported in the literature.

The structure of CNF–GA interlayer was first characterized by X-ray diffraction (XRD), X-ray photoelectron spectroscopy (XPS), Fourier transformed infrared (FTIR) spectroscopy, and scanning electron microscopy (SEM) (**Figure 1**; Figures S1–S4, Supporting Information). A plenty of oxygen-containing groups on GA can afford strong adsorption sites toward polysulfides and thus resist the shuttle effect. This is confirmed by XPS analysis. Specifically, the high-resolution C 1s spectrum can be fitted into three peaks, corresponding to the C—C (284.7 eV), C—O (286.4 eV), and C=O (288.0 eV) bonds, respectively (Figure S2b, Supporting Information).[37] The O 1s peak is also resolved into three peaks locating at 531.5, 532.4, and 533.0 eV, assigned to O=C, C—OH, and C—O—C, respectively (Figure S2c, Supporting Information).[38] These functional groups were confirmed by the FTIR spectrum (Figure S3, Supporting Information).

The GA aqueous solution was cast on the CNF networks to obtain CNF–GA composite films (Figure 1a). The pristine CNFs are with an average diameter of ≈250 nm and a smooth surface morphology (Figure 1b). After coating, a reduced interfiber spacing was observed, but the interconnected architecture of the carbon fibers was not influenced (Figure 1c). The energy dispersive X-ray (EDX) mapping images of the CNF–GA composite validate that the coating of GA on CNF is very uniform with a thickness of 13 nm (Figures S4 and S5, Supporting Information). The fine coating not only provides a large active adsorption surface but also ensures a direct contact between CNFs and GA, and thus forming a conductive trapping shield to effectively anchor the dissolved polysulfides. After the introduction of GA, no obvious change occurred in the thickness of the CNF membranes, ≈19 µm for both CNF and CNF–GA composite films (Figure 1c). The CNF–GA composite films were measured to have a very low mass loading of only ≈0.25 mg cm^{-2}.

To investigate the chemisorption ability of GA to LiPSs, density functional theory (DFT) calculations were first conducted with Li_2S_4 as a sample (**Figure 2**a). In contrast to a small binding energy of −0.39 eV between routine carbon (modeling with graphene nanoribbon (GNR) herein, Figure S6,

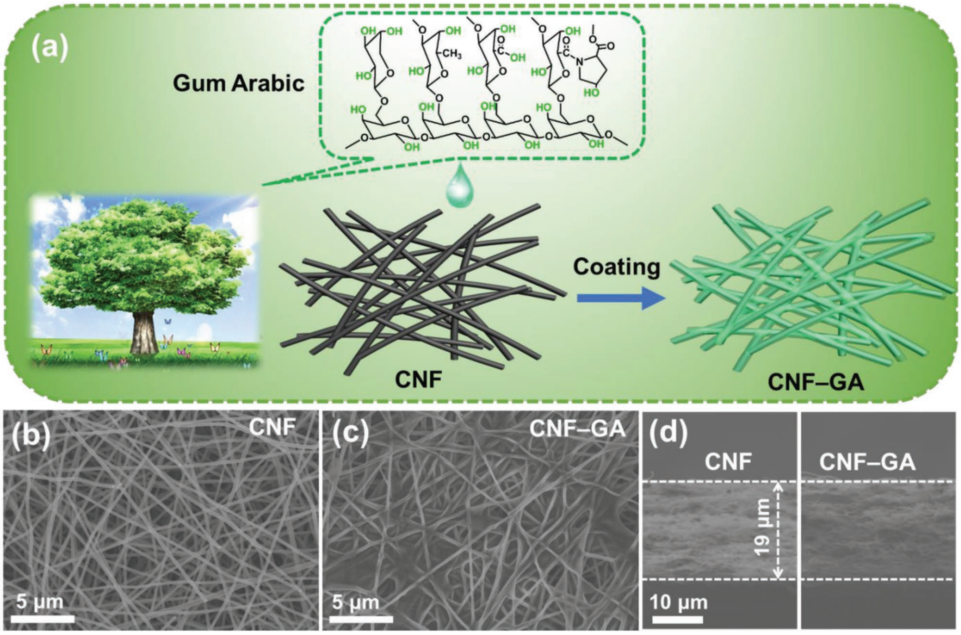

Figure 1. a) Schematic illustration of the fabrication process of the CNF–GA composite. b,c) Top-view SEM images of CNFs (b) and CNF–GA composite (c). d) Cross-sectional SEM images of the CNF membranes (left) and the CNF–GA composite films (right).

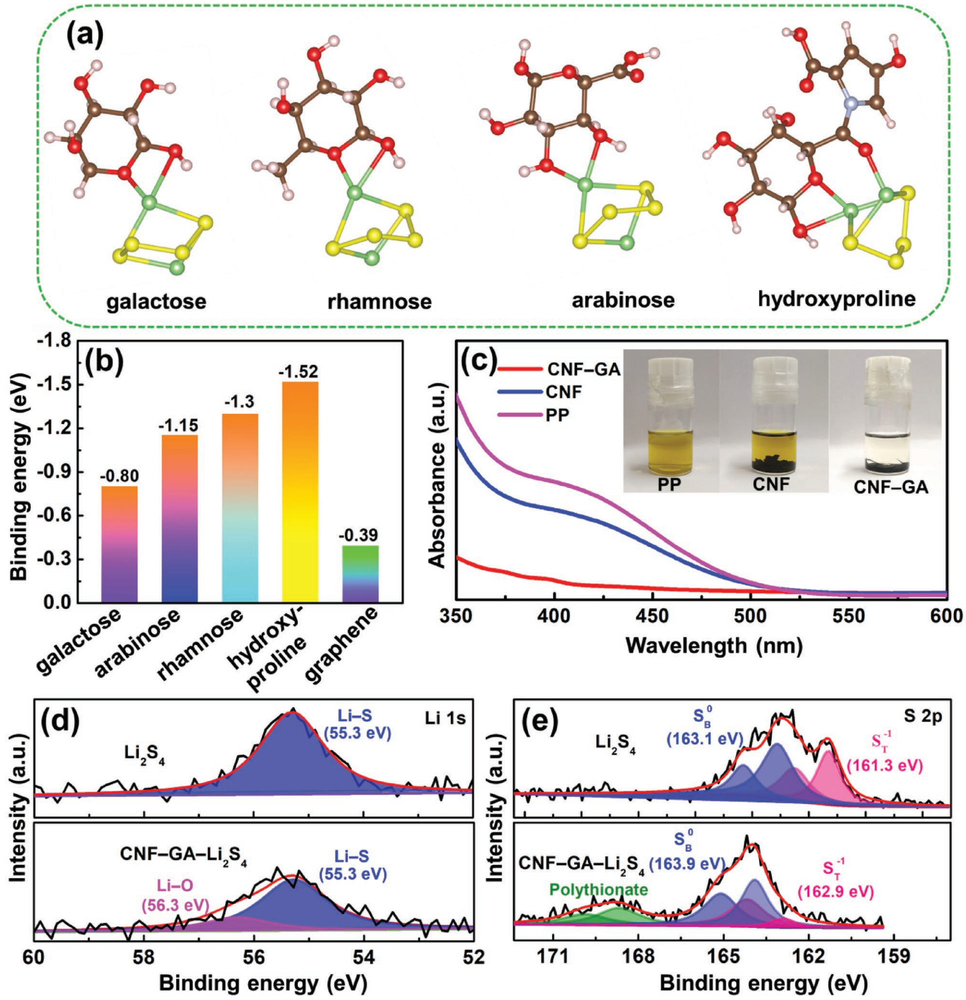

Figure 2. a) The optimized structures of four typical constitutional units of GA adsorbed with Li_2S_4. The hydrogen, lithium, carbon, nitrogen, oxygen, and sulfur are marked with white, green, brown, blue, red, and yellow. b) The summary of binding energies between Li_2S_4 and GA/graphene. c) The UV–vis spectra of the Li_2S_4 solution after exposing to the different interlayers. d,e) High-resolution XPS Li 1s and S 2p spectra before and after adsorption of Li_2S_4. The inset photographs show the Li_2S_4 solution after exposure to PP separators, CNFs, and CNF–GA composite.

Supporting Information) and Li_2S_4, the constitutional units of GA, galactose, arabinose, rhamnose, and hydroxyproline, all afford much higher binding energies of −0.80, −1.15, −1.30, and −1.52 eV, respectively (Figure 2b). The electron-rich functional in GA, such as ketone group, hydroxyl group, and cyclic oxygen, can act as the Lewis base to form a strong lithium bond with lithium polysulfides, which is consistence with our previous concept.[39,40] The formation of lithium bond is also confirmed through differential charge density analyses that electron density between lithium in LiPSs and oxygen in GA increases remarkably (Figure S7, Supporting Information).

The theoretical prediction of excellent LiPSs affinity of GA is further validated by experimental characterizations. The PP separators, CNFs, and CNF–GA composite were steeped into the Li_2S_4 solution. After 24 h dipping, no obvious color change occurred for the PP- and the CNF-containing solutions. In a sharp contrast, the yellow solution steeped with the CNF–GA composite became almost colorless, suggesting an excellent adsorptivity of GA to extract LiPSs from working electrolyte (Figure 2c). Simultaneously, UV–vis spectroscopy also validates the strong interaction between LiPSs and GA as the much weaker signal of Li_2S_4 was detected in CNF–GA-containing solutions comparing to CNF- or PP-containing solutions (Figure 2c).

The surface chemical properties of the pristine Li_2S_4 and the Li_2S_4-adsorped CNF–GA composite were investigated by XPS to further excavate the specific chemical interaction between LiPSs and GA (Figure 2d,e). Specifically, the Li 1s spectrum of the pristine Li_2S_4 displays a single symmetric peak at 55.3 eV, attributing to the formation of Li—S bond.[41] The S 2p spectrum exhibits two peaks at 161.3 and 163.1 eV, which are referred to the terminal sulfur (S_T^{-1}) and bridging sulfur (S_B^0) atoms, respectively.[42] After adsorption, the Li 1s spectrum of the CNF–GA composite was deconvoluted into two peaks. The peak at 55.3 eV is assigned to the Li—S bonds, which is the same as that of the pristine Li_2S_4. While the other one at 56.3 eV corresponds to the Li—O interaction between the polysulfides and the oxygen species of GA, definitely confirming

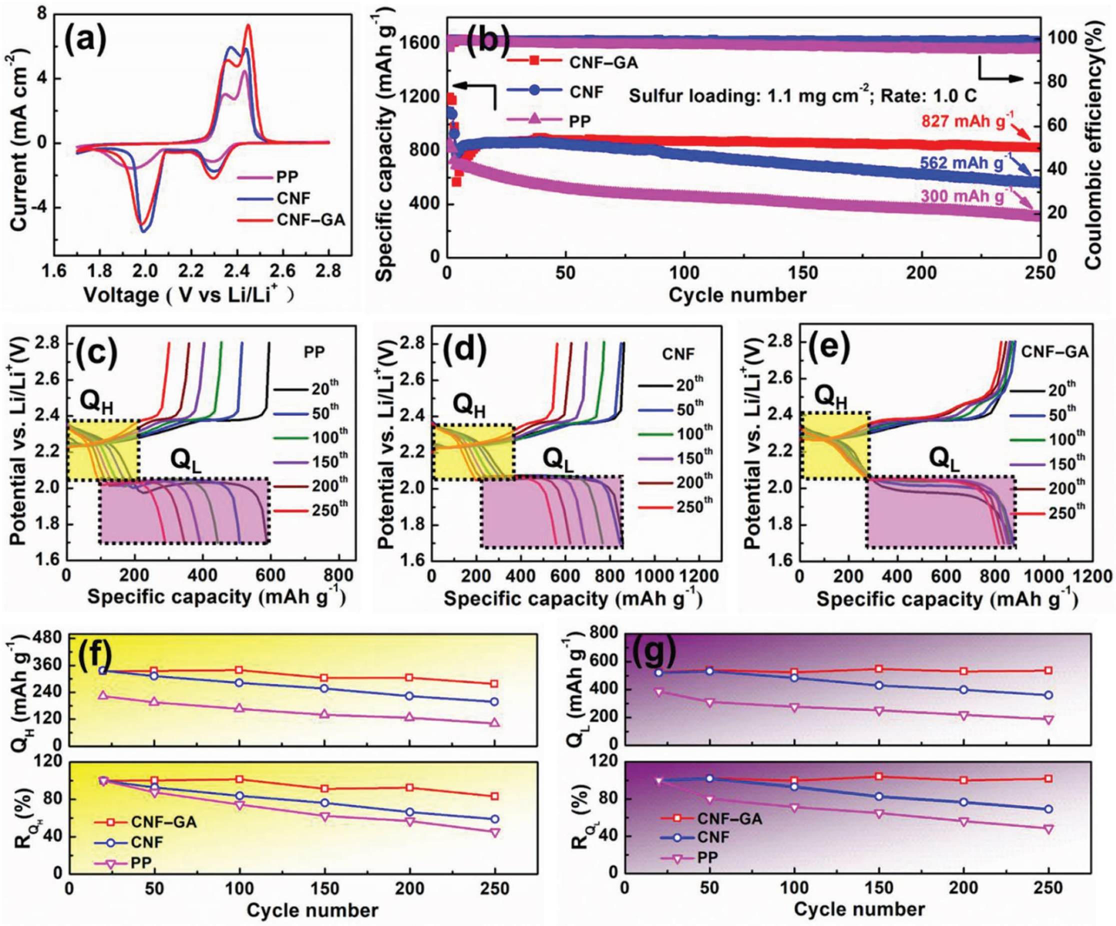

Figure 3. Electrochemical performance of Li–S batteries with different configurations. a) CV curves at a scan rate of 0.2 mV s^{-1}. b) Cycling stability at 1 C rate with a sulfur loading of 1.1 mg cm^{-2}. c–e) Charge–discharge profiles of Li–S batteries with PP (c), PP/CNF (d), and PP/CNF–GA (e) configurations at a 1.0 C current rate. f,g) The capacity fading and retention rate of the upper discharge plateaus (Q_H and R_{QH}, respectively) (f) and the lower discharge plateaus (Q_L and R_{QL}, respectively) (g) of the Li–S batteries with different configurations.

the formation of lithium bond. Similarly, the S_T^{-1} and S_B^0 peaks in the S 2p spectrum also shift to higher binding energies by 1.6 and 0.8 eV, respectively, suggesting a reduction of electron cloud density along the sulfur chains. There is no doubt that these results are attributed to the inductive effect of the electronegative oxygen atoms upon the Li—O interaction.[43,44] A pair of overlapped peaks emerge at a higher binding energy range of 168.0–170.0 eV, which are attributed to polythionates.[45] The XPS measurements confirm the strong chemical interaction between the oxygen-containing groups of GA and polysulfides.

Based on the above analysis, the CNF–GA composite is supposed to efficiently impede the shuttle effect and enhance the cycling stability of Li–S batteries. The electrochemical performance of Li–S batteries with the CNF–GA interlayers was investigated in coin cells using lithium metal anodes and 70% sulfur/carbon nanotube composite cathodes with a sulfur loading of 1.1 mg cm^{-2} (**Figure 3**). Three kinds of separator configurations were used: pure PP separators, PP/CNF membranes, and PP/CNF–GA composite films. The cyclic voltammetry (CV) curves of the three configuration cells were measured at a scanning rate of 0.2 mV s^{-1} and a potential range of 1.7–2.8 V (Figure 3a). All three configurations present a typical Li–S redox reactions. The two reduction peaks are attributed to the conversion of cyclo-S_8 to soluble long-chain polysulfides (Li_2S_n, $4 \le n \le 8$) at high potential and further reduction to short-chain polysulfides (Li_2S_n, $1 \le n < 4$). The two oxidation peaks are associated with the reversible transformation of the short-chain polysulfides to the long-chain polysulfides and cyclo-S_8.[46] Meanwhile, the cells with the CNF and CNF–GA interlayers display well-defined redox peaks with higher peak currents, indicating a rapid conversion kinetics, which is ascribed to the excellent conductivity of the CNFs. The CV curves of the cells with the CNF–GA interlayers in the first and fifth cycles shown in Figure S8 (Supporting Information) are well overlapped, confirming that the sulfur cathodes have an excellent electrochemical reversibility when integrating with the CNF–GA composite interlayers.

The cycling performance of the cells in the three kinds of configurations is evaluated at a current rate of 1.0 C (Figure 3b). The pure PP configuration delivers an initial discharge capacity of 731.7 mA h g^{-1} and drastically falls to 300 mA h g^{-1} after 250 cycles with a low Coulombic efficiency of 95%. After

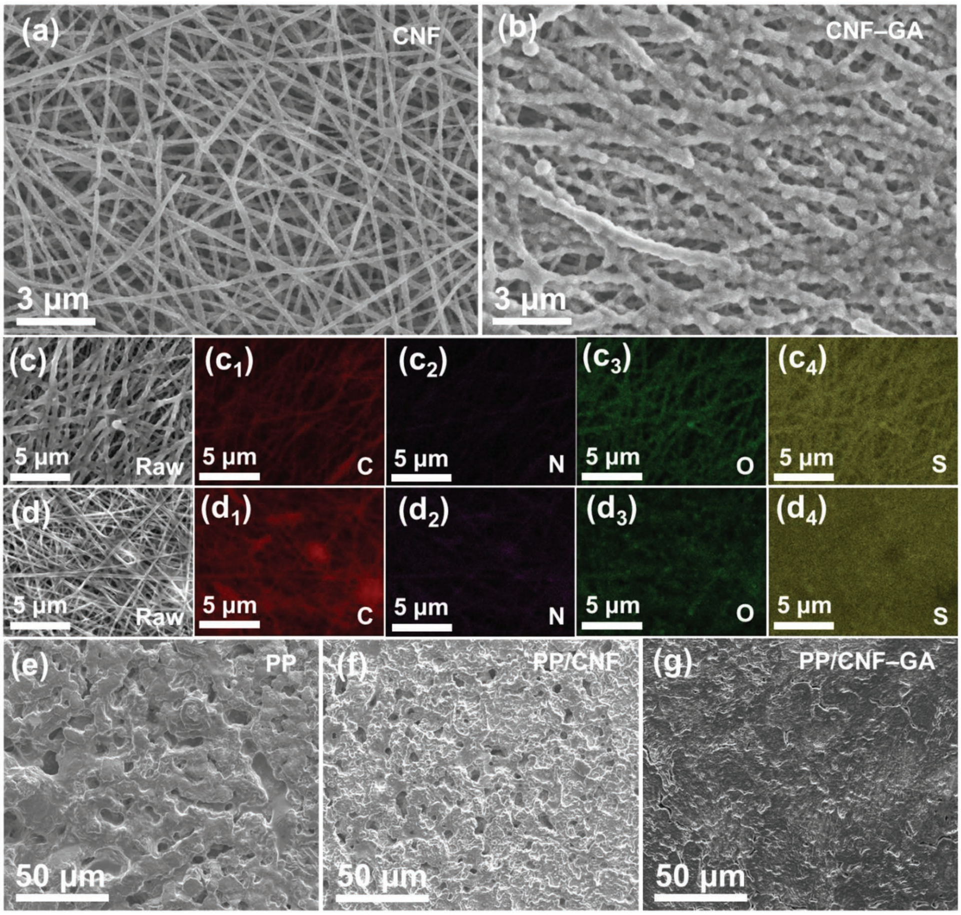

Figure 4. a,b) SEM images of CNFs (a) and CNF–GA interlayer (b) after 100 cycles at the charge state of 2.8 V. c,d) Elemental mapping images of the CNF–GA interlayers on the cathode side (c) and the PP separator side (d). e–g) SEM images of the cycled lithium metal anodes with different configurations of PP (e), PP/CNF (f), and PP/CNF–GA (g) after 100 cycles.

the introduction of the CNF interlayers, the Coulombic efficiency increases to 98% but a rapid capacity decay occurred from 870 to 562 mA h g^{-1} over 250 cycles. Surprisingly, the PP/CNF–GA configuration cells deliver a high discharge capacity of 880 mA h g^{-1} and remain 827 mA h g^{-1} after 250 cycles, demonstrating an excellent cycling stability compared with the pure PP and PP/CNF configurations. The enhanced electrochemical performance by the CNF–GA interlayers is apparently attributed to its strong chemisorption to LiPSs as affirmed above, which effectively suppresses the shuttling behavior of the soluble LiPSs and confines them in the sulfur cathode side.

The function of the GA was further investigated by analyzing the discharge–charge profiles of the Li—S cells in the three kinds of configurations (Figure 3c–e). Two pairs of distinct charge/discharge voltage plateaus represent the redox reactions between S and Li, which are the characteristics of Li–S batteries. The upper discharge plateau is attributed to the formation of soluble LiPSs, which are the origin of the shuttle effect. The lower discharge plateau is associated with the production of the insoluble sulfides of Li_2S_n (n = 1, 2), which brings up the sluggish reaction kinetic in the Li–S batteries. Note that the capacity decay is caused by the loss of the active sulfur material and the insufficient redox reaction. Therefore, the change of the plateau capacities is one important parameter to evaluate the electrochemical performance of Li–S batteries. The high- and low-voltage plateau capacities are extracted from the discharge voltage profiles, denoted as Q_H and Q_L (Figure 3f,g), respectively. The PP configuration displays a low Q_H of 223.4 mA h g^{-1} with a retention ratio (R_{QH}) of 45.2% after 250 cycles. Although a higher Q_H of 337 mA h g^{-1} was obtained for the PP/CNF configuration, it suffers a severe capacity loss after 250 cycles and only 58.3% capacity retained. In contrast, the PP/CNF–GA configuration delivers a much better stability with a high Q_H of 334 mA h g^{-1} and 83.8% retention after 250 cycles (Figure 3f). These results clearly identify that the shuttling behavior of the polysulfides was effectively suppressed by the CNF–GA interlayer. It is more distinct in the low discharge plateau region (Figure 3g). Compared with the fast capacity degradation for the PP and PP/CNF configurations, no obvious capacity loss was observed for the PP/CNF–GA configuration, indicating that the CNF–GA interlayer not only addresses the shuttling issue but also ensures a high activity and sufficient reaction of the insoluble sulfides.

The rate performance of the Li–S batteries with different configurations was probed under various current rates from

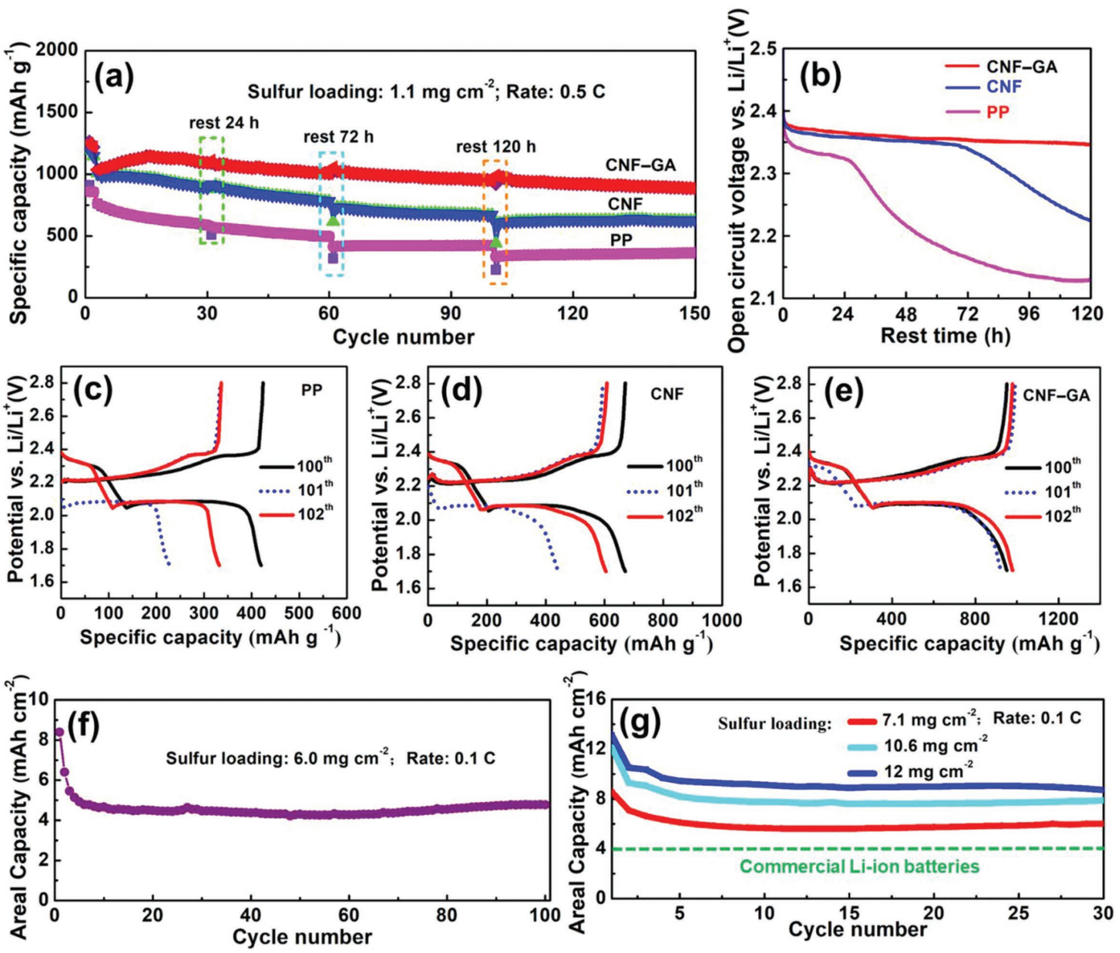

Figure 5. Self-discharge test of the Li–S batteries with different separator configurations. a) The cycling stability after different rest periods of 24, 72, and 120 h. b) The open-circuit voltage curves of the Li–S batteries during the 120 h rest. c–e) The charge–discharge curves before and after 120 h rest. f,g) Cycling performance of the high-sulfur-loading cathodes of 6 mg cm^{-2} (f) and 7.1, 10.6, and 12 mg cm^{-2} (g) in cells with the CNF–GA interlayers.

0.2 to 3.0 C (Figure S10, Supporting Information). An excellent rate capability was achieved for the PP/CNF and PP/CNF–GA configurations. It delivers discharge capacities of 1248.5, 1069.3, 884.0, 686.9, and 544.0 mA h g^{-1} for the PP/CNF configuration and 1255.7, 992.6, 818.6, 690.2, and 567.5 mA h g^{-1} for the PP/CNF–GA configuration at the current densities of 0.2, 0.5, 1.0, 2.0, and 3.0 C, respectively. A capacity of 966.2 mA h g^{-1} was recovered for the PP/CNF configuration when the current rate was changed back to 0.2 C, while it is 1058.9 mA h g^{-1} for the PP/CNF–GA configuration, suggesting that the incorporation of GA and CNFs significantly improved the reaction kinetics. However, the PP configuration underwent a poor rate performance with a capacity retention of only 527.7 mA h g^{-1} at 2.0 C, much lower than those with CNFs. The kinetics of the cells with the three kinds of configurations was further investigated using electrochemical impedance spectroscopy (EIS) (Figure S11, Supporting Information). The smallest charge transfer resistance and a steeper line in the low-frequency range are presented for the PP/CNF–GA configuration, revealing a faster Li-ion diffusion. The results are consistent with the achievements in the rate performance tests. In addition, the charge transfer resistance of the cells with CNF–GA interlayers greatly decreases along the advance of cycling, consisting with the good cycling stability.

To gain insights into the suppression function by GA, the structures and morphologies of the CNF and CNF–GA interlayers were investigated using SEM after 100 cycles. In comparison with the pristine CNFs, no obvious change in the structure was observed for the CNFs except that the surface morphology became rough after cycling. This is induced by the formation of sulfides. In contrast, the CNF–GA interlayers show an enlarged diameter of CNFs and numerous sulfur particles anchored along the CNFs (**Figure 4**a,b), clearly demonstrating the strong adsorptivity of GA to LiPSs. Furthermore, the elemental mapping was conducted on both sides of the cycled CNF–GA interlayers (Figure 4c,d). The mapping images reveal a pronounced sulfur signal with a homogeneously distribution along the CNFs on the cathode side, while the sulfur signal is very weak on the separator side, suggesting that the CNF–GA interlayer has effectively prevented LiPSs from diffusing through the interlayers and restrained them within the cathode side (Figure S12, Supporting Information). The surface morphologies of the Li metal anodes were also examined by SEM after 100 cycles with the three kinds of separator configurations (Figure 4e,f). The results show a severe surface corrosion by the diffused LiPSs for the PP and PP/CNF configurations, but no obvious corrosion and a smooth surface for the PP/CNF–GA configuration, affording further evidence to the successful inhibition of the polysulfides shuttling behavior due to the strong chemical adsorptivity of GA.

Self-discharge behavior is also a critical parameter for practical applications of Li–S batteries.[38] The self-discharge behavior of the cells with different separator configurations was investigated by detecting the changes of the open-circuit voltages (OCV) and capacities during the rest times of 24 h after 30 cycles, 48 h after 60 cycles, and 120 h after 100 cycles (**Figure 5**). After the intermittent discharge–charge tests of 150 cycles at 0.5 C, the capacities with PP and PP/CNF configurations only remained 63.0% and 47.9%, respectively. In sharp contrast, the PP/CNF–GA configuration delivers a high capacity retention of 84%. The variation of the OCVs during the 120 h rest time after 100 cycles is compared between the cells with the three kinds of separator configurations in Figure 5b. The OCVs suffered a drastic decline from ≈2.40 to 2.13 V for PP and 2.23 V for the PP/CNF configurations, respectively, while it is more stable for the PP/CNF–GA configuration with a slight decrease to 2.35 V, suggesting that the self-discharge is effectively suppressed by the CNF–GA interlayers. Similar results are displayed in the charge/discharge profiles before and after the open-circuit tests. After the 120 h rest, the high-voltage discharge plateau disappeared for the PP and PP/CNF configurations, which was companied with significant capacity loss, while the PP/CNF–GA configuration still clearly shows a typical two-plateau discharge curve with a complete capacity recovery. These reveal that GA is an effectively polysulfide-immobilizing polymer to retard the self-discharge behavior in Li–S batteries.

The Li–S batteries with higher-sulfur-loading cathodes and the CNF–GA interlayers were fabricated to evaluate the potential for practical applications. For sulfur cathodes with a high loading of 6 mg cm^{-2}, a high reversible capacity of 4.77 mA h cm^{-2} was delivered at a current rate of 0.1 C with a stable cycling over 100 cycles (Figure 5f). More intriguingly, even at higher sulfur loadings of 7.1, 10.6, and 12.0 mg cm^{-2}, the Li–S batteries can be steadily cycled up to 30 times at 0.1 C with reversible areal capacities of 7.32, 9.95, and 10.8 mA h cm^{-2}, respectively (Figure 5g). The results further show that the CNF–GA interlayers are promising for boosting the practical applications of Li–S batteries.

With all the demonstrations above, the CNF–GA composite possesses the following advantages for practical high-loading Li–S batteries. The LiPSs can easily pass through the conventional PP separator and cause severe shuttle effect and a fast performance degradation (**Figure 6**a). Although the introduction of conductive CNF interlayer can reuse of LiPSs escaping from the sulfur hosts, it can only afford a very weak immobilization on LiPSs (Figure 6b). Therefore, CNF interlayers mostly work as a physical barrier, which can physically impede the diffusion of polysulfides to some degree but cannot suppress the shuttle effects efficiently. In contrast, the CNF–GA composite interlayers afford a strong chemisorption to trap polysulfides due to the abundant oxygen-containing functional groups of GA, preventing the polysulfides from migrating to the lithium metal anodes and thus effectively suppressing the shuttle effect (Figure 6c). Simultaneously, the adsorbed polysulfides can be reused due to the excellent conductivity of CNF–GA network. Besides, the as-obtained CNF–GA interlayer is cheap and easy to synthesized, meeting the requirements of practical Li–S batteries.

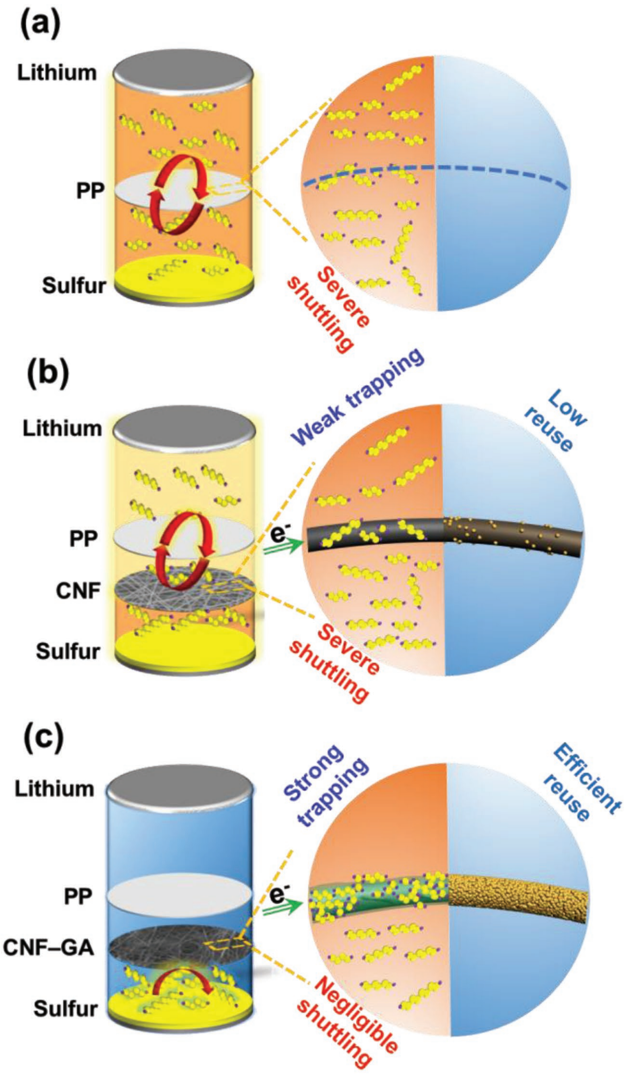

Figure 6. a–c) Schematic illustration of the operation of the Li–S batteries with different configurations of PP (a), PP/CNF (b), and PP/CNF–GA (c).

In conclusion, a polysulfide-immobilizing polymer interlayer was prepared through coating a nature polymer of GA on a conductive CNF membrane for Li–S batteries. Benefiting from the abundant oxygen-containing functional groups, GA can afford a strong chemical interaction toward polysulfides and thereby effectively suppress the shuttling behavior. Along with the good conductivity of the CNFs, an efficient reuse of the adsorbed sulfides was realized and thus a high utilization of sulfur. As a result, the sulfur cathodes with the CNF–GA interlayers demonstrated an outstanding electrochemical performance with a high discharge specific capacity of 880 mA h g^{-1} and a high retention of 827 mA h g^{-1} after 250 cycles at 1.0 C. Even at a high sulfur loading up to 12 mg cm^{-2}, a stable cycling was achieved with a reversible areal capacity of 10.8 mA h cm^{-2}.

In combination with the nature source of GA, the simple fabrication process and the excellent performance, our findings provide a promising strategy to develop viable Li–S batteries for practical applications.

Supporting Information

Supporting Information is available from the Wiley Online Library or from the author.

Acknowledgements

The authors acknowledge the financial support from the National Natural Science Foundation of China (Grant Nos. 51672188 and 21676160), Natural Science Foundation of Tianjin City (Grant No. 16JCYBJC40900) and National Key Research and Development Program (Grant No. 2016YFA0202500), and the support from Tsinghua National Laboratory for Information Science and Technology for theoretical simulations. Y.H.X. acknowledges the Thousand Talents Plan for Young Professionals of China.

Conflict of Interest

The authors declare no conflict of interest.

Keywords

Gum Arabic, high sulfur loading, lithium–sulfur batteries, polysulfide-immobilizing polymers, shuttle effect

Received: July 17, 2018
Revised: August 23, 2018

---

[1] P. G. Bruce, S. A. Freunberger, L. J. Hardwick, J.-M. Tarascon, *Nat. Mater.* **2012**, *11*, 19.
[2] H. F. Shi, W. Lv, C. Zhang, D. W. Wang, G. W. Ling, Y. B. He, F. Y. Kang, Q. H. Yang, *Adv. Funct. Mater.* **2018**, *28*, 1800508.
[3] A. Manthiram, Y. Z. Fu, S. H. Chung, C. X. Zu, Y. S. Su, *Chem. Rev.* **2014**, *114*, 11751.
[4] H. J. Peng, J. Q. Huang, X. B. Cheng, Q. Zhang, *Adv. Energy Mater.* **2017**, *7*, 1700260.
[5] Y. V. Mikhaylik, J. R. Akridge, *J. Electrochem. Soc.* **2004**, *151*, A1969.
[6] S. S. Zhang, *J. Power Sources* **2013**, *231*, 153.
[7] X. L. Ji, K. T. Lee, L. F. Nazar, *Nat. Mater.* **2009**, *8*, 500.
[8] T. H. Zhou, W. Lv, J. Li, G. M. Zhou, Y. Zhao, S. X. Fan, B. L. Liu, B. H. Li, F. Y. Kang, Q. H. Yang, *Energy Environ. Sci.* **2017**, *10*, 1694.
[9] Y. H. Xu, Y. Wen, Y. J. Zhu, K. Gaskell, K. A. Cychosz, B. Eichhorn, K. Xu, C. S. Wang, *Adv. Funct. Mater.* **2015**, *25*, 4312.
[10] S. Xin, L. Gu, N. H. Zhao, Y.-X. Yin, L.-J. Zhou, Y.-G. Guo, L.-J. Wan, *J. Am. Chem. Soc.* **2012**, *134*, 18510.
[11] J. L. Wang, J. Yang, J. Y. Xie, N. X. Xu, *Adv. Mater.* **2002**, *14*, 13.
[12] N. Jayaprakash, J. Shen, S. S. Moganty, A. Corona, L. A. Archer, *Angew. Chem.* **2011**, *123*, 6026.
[13] Z. H. Sun, J. Q. Zhang, L. C. Yin, G. J. Hu, R. P. Fang, H.-M. Cheng, F. Li, *Nat. Commun.* **2017**, *8*, 14627.
[14] C. Luo, W. Lv, Y. Q. Deng, G. M. Zhou, Z.-Z. Pan, S. Z. Niu, B. H. Li, F. Y. Kang, Q.-H. Yang, *Small* **2017**, *13*, 1700358.
[15] N. Wang, Z. F. Xu, X. Xu, T. Liao, B. Tang, Z. C. Bai, S. X. Dou, *ACS Appl. Mater. Interfaces* **2018**, *10*, 13573.
[16] S. S. Zhang, *Electrochim. Acta.* **2012**, *70*, 344.
[17] X. Y. Yao, N. Huang, F. D. Han, Q. Zhang, H. L. Wan, J. P. Mwizerwa, C. S. Wang, X. X. Xu, *Adv. Energy Mater.* **2017**, *7*, 1602923.
[18] T. Gao, X. Ji, S. Hou, X. L. Fan, X. G. Li, C. Y. Yang, F. D. Han, F. Wang, J. J. Jiang, K. Xu, C. S. Wang, *Adv. Mater.* **2018**, *30*, 1704313.
[19] J. L. Wang, Z. D. Yao, C. W. Monroe, J. Yang, Y. N. Nuli, *Adv. Funct. Mater.* **2013**, *23*, 1194.
[20] F. L. Zeng, W. K. Wang, A. B. Wang, K. G. Yuan, Z. Q. Jin, Y.-S. Yang, *ACS Appl. Mater. Interfaces* **2015**, *7*, 26257.
[21] W. Chen, T. Y. Lei, T. Qian, W. Q. Lv, W. D. He, C. Y. Wu, X. J. Liu, J. Liu, B. Chen, C. L. Yan, J. Xiong, *Adv. Energy Mater.* **2018**, *8*, 1702889.
[22] Q. W. Lu, Y.-B. He, Q. P. Yu, B. H. Li, Y. V. Kaneti, Y. W. Yao, F. Y. Kang, Q.-H. Yang, *Adv. Mater.* **2017**, *29*, 1604460.
[23] S. Liu, A. X. Wang, Q. Q. Li, J. S. Wu, K. Chiou, J. X. Huang, J. Y. Luo, *Joule* **2018**, *2*, 184.
[24] N.-W. Li, Y. Shi, Y.-X. Yin, X.-X. Zeng, J.-Y. Li, C.-J. Li, L.-J. Wan, R. Wen, Y.-G. Guo, *Angew. Chem., Int. Ed.* **2018**, *57*, 1505.
[25] X.-Q. Zhang, X. Chen, X.-B. Cheng, B.-Q. Li, X. Shen, C. Yan, J.-Q. Huang, Q. Zhang, *Angew. Chem., Int. Ed.* **2018**, *57*, 5301.
[26] Y. Y. Liu, Y.-K. Tzeng, D. C. Lin, A. Pei, H. Lu, N. A. Melosh, Z.-X. Shen, S. Chu, Y. Cui, *Joule* **2018**, *2*, 1.
[27] Y.-S. Su, A. Manthiram, *Chem. Commun.* **2012**, *48*, 8817.
[28] Z. Q. Jin, K. Xie, X. B. Hong, Z. Q. Hu, X. Liu, *J. Power Sources* **2012**, *218*, 163.
[29] J.-Q. Huang, Q. Zhang, H.-J. Peng, X.-Y. Liu, W.-Z. Qian, F. Wei, *Energy Environ. Sci.* **2014**, *7*, 347.
[30] S. Y. Bai, X. Z. Liu, K. Zhu, S. C. Wu, H. S. Zhou, *Nat. Energy* **2016**, *1*, 16094.
[31] Z. Z. Du, C. K. Guo, L. J. Wang, A. J. Hu, S. Jin, T. M. Zhang, H. C. Jin, Z. K. Qi, S. Xin, X. H. Kong, Y.-G. Guo, H. X. Ji, L.-J. Wan, *ACS Appl. Mater. Interfaces* **2017**, *9*, 43696.
[32] P.-Y. Zhai, H.-J. Peng, X.-B. Cheng, L. Zhu, J.-Q. Huang, W. C. Zhu, Q. Zhang, *Energy Storage Mater.* **2017**, *7*, 56.
[33] F. Pei, L. L. Lin, A. Fu, S. G. Mo, D. H. Ou, X. L. Fang, N. F. Zheng, *Joule* **2018**, *2*, 323.
[34] H. Espinosa-Andrews, J. G. Baez-Gonzalez, F. Cruz-Sosa, E. J. Vernon Carter, *Biomacromolecules* **2007**, *8*, 1313.
[35] G. R. Li, M. Ling, Y. F. Ye, Z. P. Li, J. H. Guo, Y. F. Yao, J. F. Zhu, Z. Lin, S. Q. Zhang, *Adv. Energy Mater.* **2015**, *5*, 1500878.
[36] Y. L. Chen, N. Q. Liu, H. Y. Shao, W. K. Wang, M. Y. Gao, C. M. Li, H. Zhang, A. B. Wang, Y. Q. Huang, *J. Mater. Chem. A* **2015**, *3*, 15235.
[37] M. F. Chen, S. X. Jiang, C. Huang, X. Y. Wang, S. Y. Cai, K. X. Xiang, Y. P. Zhang, J. X. Xue, *ChemSusChem* **2017**, *10*, 1803.
[38] Y. Pang, J. S. Wei, Y. G. Wang, Y. Y. Xia, *Adv. Energy Mater.* **2018**, *8*, 1702288.
[39] T.-Z. Hou, X. Chen, H.-J. Peng, J.-Q. Huang, B.-Q. Li, Q. Zhang, B. Li, *Small* **2016**, *12*, 3283.
[40] J. Xie, H.-J. Peng, J.-Q. Huang, W.-T. Xu, X. Chen, Q. Zhang, *Angew. Chem., Int. Ed.* **2017**, *56*, 16223.
[41] H.-J. Peng, Z.-W. Zhang, J.-Q. Huang, G. Zhang, J. Xie, W.-T. Xu, J.-L. Shi, X. Chen, X.-B. Cheng, Q. Zhang, *Adv. Mater.* **2016**, *28*, 955.
[42] Z. W. Seh, H. T. Wang, P.-C. Hsu, Q. F. Zhang, W. Y. Li, G. Y. Zheng, H. B. Yao, Y. Cui, *Energy Environ. Sci.* **2014**, *7*, 672.
[43] Q. Pang, J. T. Tang, H. Huang, X. Liang, C. Hart, K. C. Tam, L. F. Nazar, *Adv. Mater.* **2015**, *27*, 602.
[44] G. R. Li, W. Lei, D. Luo, Y.-P. Deng, D. L. Wang, Z. W. Chen, *Adv. Energy Mater.* **2017**, *8*, 1702381.
[45] X. Liang, C. Hart, Q. Pang, A. Garsuch, T. Weiss, L. F. Nazar, *Nat. Commun.* **2015**, *6*, 5682.
[46] T. Chen, B. R. Cheng, G. Y. Zhu, R. P. Chen, Y. Hu, L. B. Ma, H. L. Lv, Y. R. Wang, J. Liang, Z. X. Tie, Z. Jin, J. Liu, *Nano Lett.* **2017**, *17*, 437.